JOURNAL OF SOLID STATE CHEMISTRY 79, 218–231 (1989)

Stability of Phases $CaZrO_3$ and $CaZr_4O_9$ Incorporated in the System $CaO–ZrO_2$

ANURAG DWIVEDI AND A. N. CORMACK

NYS College of Ceramics, Alfred University, Alfred, New York 14802

Received October 7, 1988; in revised form December 19, 1988

Zirconia-based solid electrolytes are among the best known oxygen–ion conductors. During the last few decades, efforts have been made to understand the behavior of transport properties in stabilized zirconia. Recent investigations show that defect interactions, defect clustering and ordering, and microdomain formation all play an important role in the transport properties of stabilized zirconias. Further investigation is, however, required to understand the effect of defects, their interaction and ordering on transport, and related properties of stabilized zirconia systems. A degradation in properties due to aging phenomena in stabilized zirconias has been found. Recent studies reveal the presence of phases $CaZrO_3$ and $CaZr_4O_9$ in aged stabilized zirconia. In the present investigation, our main interest is in examining the formation and stability of the phases $CaZrO_3$ and $CaZr_4O_9$ in calcia-stabilized zirconia. We studied the energetics of these phases and calculated the relaxed ionic coordinates by atomistic computer simulation techniques.

1. Introduction

The most recent $CaO–ZrO_2$ phase diagram, presented by Hellmann and Stubican (*1*), includes distinct $CaZr_4O_9$ and $CaZrO_3$ phase fields (Fig. 1). Typically about 13 mole% CaO is added to stabilize the zirconia completely. Such a high concentration of dopant in combination with the same number of compensating anion vacancies gives rise to a highly defective system. In these circumstances, defect complexes and ordered phases are likely to occur. The formation of ordered phases in this material has frequently been discussed in the literature (*2*), and the presence of such phases has been suggested to lead to the deterioration of the electrical and mechanical properties of stabilized zirconia.

The conductivity studies of Tien and Subbarao (*2*), among others, show that the conductivity of calcia-stabilized zirconia (CSZ) decreases as CaO content is increased from 13 to 20 mole%. Baumard and Abelard (*3*) plotted the ionic conductivities as a function of dopant concentration for different stabilized zirconia systems. The conductivity in all of these cases shows a maxima at a certain composition (mostly near the lower cubic phase boundary). The apparent anomalous behavior of the conductivity in this system is believed to be due to (a) the interactions between the charged defects (dopant and charge compensating vacancies) and (b) the formation of ordered phases. Several studies have been done to understand the nature and structure of interacting defects and ordered phases but still the problem seems to be unresolved.

0022-4596/89 $3.00

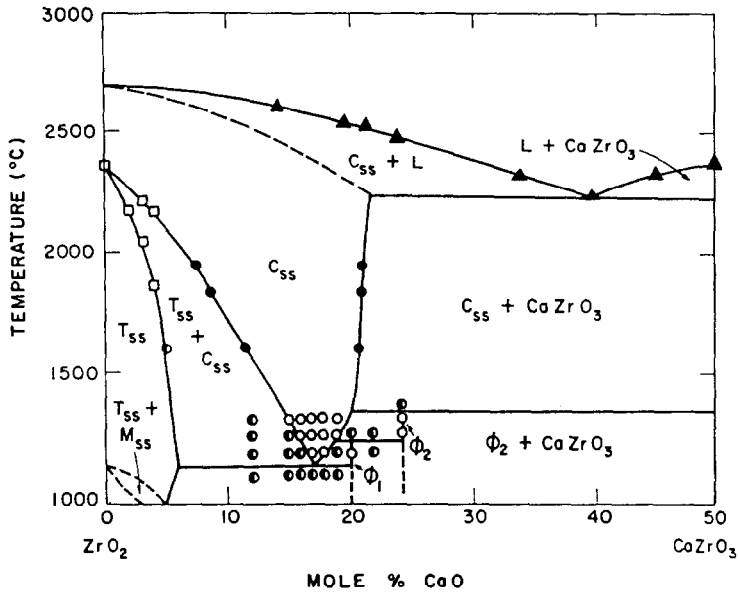

FIG. 1. CaO–ZrO_2 phase diagram [taken from Ref. (*1*)].

Tien and Subbarao (*2*) observed a reversible order–disorder transition in the ZrO_2–CaO system by XRD and by repeated annealing and conductivity measurements. The conductivity in ordered samples was found to be lower than that of disordered samples, which led them to conclude that anion vacancies assume ordered sites instead of being randomly distributed. Subbarao proposed that the Ca^{2+} ions also assume ordered cation sites. The ordered Ca^{2+} ions, according to Tien and Subbarao (*2*), attract anion vacancies to the nearest-neighbor (nn) positions due to coulombic forces. Thus, because of ordering of Ca_{Zr}, the anion vacancies become ordered, leading to decreased ionic conductivities.

The diffuse scattering and forbidden reflections observed in neutron diffraction studies of CSZ prompted Carter and Roth (*4*) to propose that the high-temperature disordered state of CSZ has a cubic fluorite structure with oxygen ions displaced from the ideal fluorite lattice sites and that the low-temperature (<1300°K) ordered state involved cooperative ordering of the oxygen ions and vacancies on the oxygen sublattice. Bacquet *et al.* (*5*) investigated the paramagnetic resonance spectra of Gd^{3+} and Yb^{3+} in annealed single crystals of CSZ in the *X* band. In both cases, sites of almost cubic symmetry with a weak axial deformation, the principal axis of which is directed along a ⟨100⟩ direction, were observed. These results supported the conclusions of Carter and Roth (*4*) concerning the existence of an order–disorder transformation of CSZ by annealing at 1000°C, and confirmed the ordered arrangement that Carter and Roth had proposed for the O^{2-} ions around the zirconium sites. The atomic arrangement and the presence of Ca^{2+} ions and oxygen vacancies near the defects could account for the anomalous linewidth observed, according to their model.

Allpress *et al.* (*6*) inferred from their electron diffraction studies that, at lower temperatures, domains of an ordered arrangement (about 3 nm in diameter) exist, embedded coherently in a cubic matrix.

Similar work by Hudson and Moseley (*7*) demonstrated that the intensity of diffuse scattering increases with CaO content, while the intensity of extra (forbidden) reflections decreases with CaO content. This suggested that anion vacancies become aligned along ⟨111⟩ directions. Allpress *et al.* (*6*) further reported the presence of coherent microdomains of $CaZr_4O_9$ (analogous to the $CaHf_4O_9$ phase found in the corresponding $CaO–HfO_2$ system) and intragranular precipitates of monoclinic zirconia in a cubic matrix, as a result of aging.

Faber *et al.* (*9*) refined the neutron diffraction studies on CSZ and yttria-stabilized zirconia (YSZ). They found that the oxygen ions were shifted from the ideal fluorite positions (by about 0.023 nm) by an internal shear deformation of the oxygen sublattice. This may (as in CSZ) or may not (as in YSZ see also ref. (*8*)) be accompanied by external strain.

Moringa *et al.* (*10, 11*) from their X-ray diffuse scattering results deduced that oxygen ion displacements occur preferentially along ⟨100⟩ directions in the fluorite lattice but without long-range correlation. Displacement terms in the diffuse scattering, which tend to dominate in the scattering measurements, clearly show that the elastic energy is minimized by anion lattice relaxation around the oxygen vacancies. These experiments suggested that the oxygen vacancies tend to associate with Ca^{2+} ions, i.e., $Ca_{Zr}–V_O$ interactions were predominantly nn interactions.

The most recent experimental technique to be applied to the question of whether the charge-compensating oxygen vacancies sit in the nn site to the dopant, either for Ca^{2+} with which we are concerned here or for a trivalent ion such as Y^{3+}, is EXAFS (extended X-ray absorption fine structure). This technique probes the local structure around a particular ion; however, the analysis of EXAFS data is not always straightforward. This is highlighted by the fact that separate studies have yielded different interpretations. Goldman *et al.* (*12*) conclude from their data, at least in trivalent-doped zirconia, that the vacancy occupies a nn site. On the other hand, Moroney and coworkers (*13, 14*) have deduced a next-nearest-neighbor (nnn) position for the vacancy in YSZ, based on the fact that amplitude of the Zr–O shell is less than that of the Y–O shell. In this case, computer simulations also indicate a preference for nnn oxygen vacancies (*14, 15*).

In a related computational study on CSZ, reported in detail elsewhere (*16, 17*), we concluded that a nnn position was favored as well, although the situation is less clear cut than for YSZ. An EXAFS study of CSZ (*18*) indicates a more complex structure around the Ca^{2+} dopant ions than around Y^{3+} ions in YSZ although the Zr EXAFS and fourier-transformed data are very similar to that from the YSZ, suggesting a similar environment for Zr in both cases. The inference is thus for a nnn site for the oxygen vacancy in both cases. The interpretation is, however, less certain in the case of CSZ.

Various experimental results on CSZ and other heterovalent-doped zirconia, e.g., the results of Stubican and Corman (*19*), show also that the ionic diffusion and conduction decreases with increasing defect concentration, where the activation energy of the mobility is increased.

Notwithstanding the controversy of whether the V_O is in the nn or nnn site with respect to the Ca dopant, it is clear that there are substantial interactions between the two kinds of point defects which lead to the formation of larger defect complexes and ultimately to the precipitation of other phases in the system. The presence of $CaZrO_3$ at high CaO concentration is well established, and there is increasing evidence for the existence of the phase $CaZr_4O_9$. The work of Hellmann and Stubican (*1*) indicates that the very long anneal-

ing time needed in their study is the reason why this phase was not seen in earlier studies.

The formation of phases $CaZrO_3$ and $CaZr_4O_9$ is reported to degrade the properties of stabilized zirconia with time. In this paper, we report a study of lattice and defect energies in the phases $CaZrO_3$ and $CaZr_4O_9$ calculated with the intention that they may reveal the aging phenomena and the microdomain formation in the present system. The calculations were performed to confirm the formation and stability of phases $CaZrO_3$ and $CaZr_4O_9$. By analogy with the structural analysis of $CaHf_4O_9$, our calculations suggest that in the $CaZr_4O_9$ phase, the anion vacancies get ordered in such a way that they are always at nnn positions to the Ca^{2+} ions; this is consistent with our previous results, reported elsewhere (*16, 17*), regarding the defect structure and defect interactions in CaO-stabilized zirconia system. In addition, we suggest that the formation of the $CaZr_4O_9$ phase is a natural consequence of the continued long-range interaction between point defects to form an ordered stoichiometric superlattice phase.

2. Computational Techniques

In this section, the computation techniques and procedures used in the present study are discussed. The calculations, based on the Born model, employ interatomic potential models and thus the reliability of the simulations will be dependent on the validity of these potential models. We previously demonstrated the viability of the model we use here (*16, 17*). Brief descriptions of the interatomic potentials used and lattice energy and defect energy calculations performed are given next.

2.1. Potential Models

In the present study, the potentials used are based on the Born model with integral ionic charges. The central-force, pairwise, short-range potentials are described, as usual, by a simple analytical function, most commonly the Born–Mayer potential, supplemented by an attractive r^{-6} term, i.e.,

$$V_{ij}(r_{ij}) = A_{ij} \exp(-r_{ij}/\rho) - C_{ij}r_{ij}^{-6}. \quad (1)$$

The polarizability of individual ions is included by the shell model of Dick and Overhauser (*20*) in which the outer valence electron cloud is simulated by a massless shell of charge Y and the nucleus and the inner electrons by a core of charge X. The total charge of the ion is, thus, $X + Y$, which is set equal to the oxidation state of the ion. The interaction between core and shell of any ion is assumed to be harmonic and is given by

$$V_i(r_i) = \tfrac{1}{2}k_i r_i^2. \quad (2)$$

For the shell model the value of the free-ion electronic polarizability is given by the expression:

$$\alpha_i = (Y_i)^2/k_i. \quad (3)$$

The potential parameters A, ρ, and C in Eq. (1), and the shell charges, Y, and spring constant, k, associated with shell-model description of polarizability were derived by the procedure of "empirical fitting," i.e., these parameters were adjusted by a least-squares fitting routine, so as to achieve the best possible agreement between calculated and experimentally observed crystal properties (*16*).

A crucial feature of zirconia is that the cubic fluorite structured phase is not stable at lower temperatures, the standard explanation being that the radius of the zirconium cation is too small for eightfold cubic coordination and hence the lower symmetry distortions that occur as the oxygens pack more closely around the zirconium cation. In interatomic potential terms, this means that if the potential is derived by fitting to the fluorite structure, then the model will include a cation radius that is too large

TABLE I

POTENTIAL PARAMETERS USED IN THE PRESENT STUDY

Interaction	A	ρ	C
Ca–O[a]	1,090.400	0.344	0.000
Zr–O	985.869	0.376	0.000
O–O	22,764.300	0.149	27.890

Note. Potential form: $V(r) = A \exp(-r/\rho) - Cr^{-6}$.
[a] Potentials taken from Lewis and Catlow (*22*).

and this error will be built into the predictions from the calculations. Moreover, that approach assumes that the cubic structure is the equilibrium one, and hence any defect calculations done on the lower symmetry structures will incorporate a fictitious relaxation energy term, since the structure around the defect will try to regain its cubic configuration (*21*). This problem may, however, be overcome by fitting the potential parameters to both cubic and tetragonal structures. The potential parameters used in the present study are listed in Tables I and II.

2.2. *Lattice Energy Calculations*

In order to obtain the equilibrium structure, the lattice energy is minimized with respect to the atomic coordinates and lattice vectors. The lattice energy is the binding or cohesive energy of the perfect crystal per unit cell and is calculated using the Born model of the solid, from the relation

$$U = \tfrac{1}{2} \sum_i \sum_j V_{ij}, \qquad (4)$$

TABLE II

SHELL-MODEL PARAMETERS

Interaction	Shell charge (Y)	Spring constant (k)
Zr(Core)–Zr(Shell)	1.350	169.617
Ca(Core)–Ca(Shell)[a]	0.000	∞
O(Core)–O(Shell)	−2.077	27.290

[a] Potentials taken from Lewis and Catlow (*22*)

where the total pairwise interatomic potential, V_{ij}, is given by

$$V_{ij}(r_{ij}) = q_i q_i / r_{ij} + A_{ij} \exp(-r_{ij}/\rho_{ij}) - C_{ij} r_{ij}^{-6} \qquad (5)$$

with the first term representing the coulombic interactions between species i and j and the last two the noncoulombic short-range contributions.

Calculation of the equilibrium atomic configuration involves adjusting the coordinates until the internal basis strains (i.e., the net forces acting on a species) are totally removed. This is equivalent to minimizing the lattice energy as a function of atomic coordinates and is done using a second derivative method. For complete structural equilibration, the lattice vectors are also relaxed, using elasticity theory. Details of the procedure have been given by Cormack (*23*) and Parker (*24*).

2.3. *Defect Energy Calculations*

The defect formation energy is the energy to create a defect within the perfect lattice. The most convenient general formulation for treating the defective lattice is that developed by Norgett and Lidiard (*25*). It is based on the notion that the total energy of the system is minimized by a relaxation of the ions surrounding a defect and that the relaxation decreases fairly rapidly for distances away from the defect. As a result, the crystal can be formally partitioned into an inner region I, in which the lattice configuration is evaluated explicitly, and an outer region II, which can be viewed from the defect as a continuum, within which the displacements can be calculated on the basis of some suitable approximation (Fig. 2). In this outer region (region II) the displacements are due solely to the polarization field produced by the net charge of the defect, centered at the defect origin. For the outer region the method of Mott and Littleton is employed (see ref. *21*)

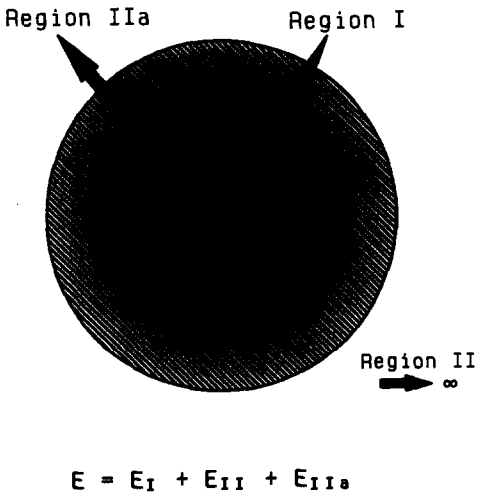

FIG. 2. Two region strategy for defect energy calculations.

which relates the polarization P to distance R, and is given by

$$P = \frac{1}{4\pi}\left(1 - \frac{1}{\varepsilon_0}\right)\frac{ZeR}{R^3} \qquad (6)$$

with ε_0 being the static dielectric constant of the material.

An interfacial region is introduced in order to account consistently for the different treatment of the two regions. This approach has been found to provide adequately for the considerable relaxation of the crystal structure around the defect. Clearly, any theoretical treatment in which the relaxation effect is not considered will show some error.

Quite formally, then, the total energy of the system is written as

$$E = E_I(x) + E_{II_a}(x, t) + E_{II}(t) \qquad (7)$$

in which the first term is the energy of the inner region, the second term the interaction energy between regions I and II, and the third term the energy of the outer region. In Eq. (7), x is a vector of independent coordinates describing the inner region, while t is a corresponding vector of the displacements in the outer region and is both formally distinguished from x and assumed to be an implicit function of it. The defect energy, E, is found by the minimization of the energy. Detailed information about theoretical methods and computer modeling of solids is given in Refs. (*24, 26–28*).

3. Results and Discussion

The techniques described in Section 2 were employed to calculate the relaxed ionic coordinates and energetics of the phases $CaZr_4O_9$ and $CaZrO_3$. $CaZr_4O_9$ is a superlattice of the ideal fluorite cubic lattice. The relation of the similar superlattice $CaHf_4O_9$ with the ideal fluorite unit cell has been reported by Allpress *et al.* (*6*); this allowed us to set up a similar type of setup for $CaZr_4O_9$ to start with. $CaZrO_3$ is another stoichiometric phase frequently seen in aged CSZ. The studies on lattice and defect energies in the phases $CaZr_4O_9$ and $CaZrO_3$ were performed with the intention that they may reveal aging phenomena and microdomain formation in the present system.

3.1. Phase $CaZr_4O_9$

The precise crystal structure of $CaZr_4O_9$ has not been reported in the literature. However, the XRD studies of similar phases in the system HfO_2–CaO by Allpress *et al.* (*6*) have enabled us to generate a preliminary structure for $CaZr_4O_9$, which may be thought of as a superstructure derived from the fluorite structure by the ordering of the calcium ions and charge-compensating oxygen vacancies.

The X-ray results of Allpress *et al.* (*6*) in the similar system $CaHf_4O_9$ indicate that during ordering, the calcium ions are always eightfold coordinated, while the smaller hafnium ions may be six-, seven-, or eightfold coordinated. This is consistent with our calculations of defect structures in the system CaO-stabilized zirconia reported elsewhere (*16, 17*) where the cal-

TABLE III

TYPE AND DIMENSIONS OF UNIT CELL OF SUPERLATTICE $CaZr_4O_9$

	$CaHf_4O_9$ (6)	$CaZr_4O_9$ (Present study)
Space group	$C_{2/c}$ Monoclinic	$C_{2/c}$ Monoclinic
Unit cell dimensions		
a (Å)	17.698_2	17.835
b (Å)	14.500_1	14.739
c (Å)	12.021_1	12.127
β (°)	119.468_6	122.840
Relation to fluorite cell	$a = [222]_f$ $b = [\bar{2}20]_f$ $c = \frac{1}{2}[33\bar{2}]_f$	

Note. Based on the work of Allpress *et al.* (6).

cium ions are found energetically stable in the eightfold coordination in preference to a lower coordination. In other words, the $CaZr_4O_9$ superlattice may be thought of as the result of ordering $[Ca_{Zr} \cdot V_O]$ defect pairs.

Given a set of coordinates for $CaZr_4O_9$, generated from its relation with the fluorite cell, as determined by Allpress *et al.* (6) for the similar phase $CaHf_4O_9$, a minimum energy equilibrium structure can be obtained by using an appropriate interatomic potential model. The initial unit cell dimensions of our model $CaZr_4O_9$ were taken from Allpress *et al.* (6) and are given in Table III along with its relation to the fluorite unit cell of ZrO_2.

The unit cell contains 16 Ca^{2+} ions, 64 Zr^{4+} ions, and 144 O^{2-} ions (16 oxygen sites out of total 160 are vacant) for a total of 224 ions, preliminary setup of which is given in Figs. 3 to 10 for various planes corresponding to different values of b_ϕ. Note that the origin of the unit cell given by Allpress *et al.* (6) differs from that in our model unit cell. This is simply because they chose a center of symmetry as the origin whereas we chose an oxygen ion, as shown in Fig. 3.

Because the unit cell is so big, to check that no error had been introduced into such a large structural setup, we initially obtained the lattice energy per formula unit of ZrO_2 from the superlattice before incorporating the Ca ions and oxygen vacancies (which comes out to be -109.68 eV) compared with that from the simple fluorite unit cell (-109.70 eV). Our supercell had thus

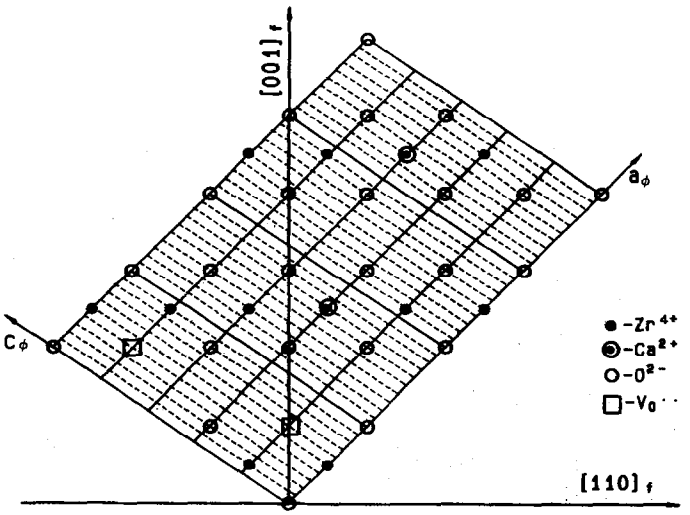

FIG. 3. Superlattice plane $b_\phi = 0.000$.

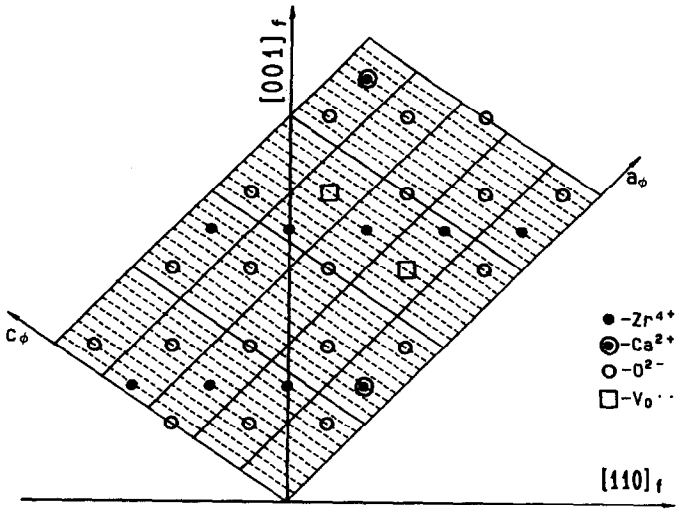

FIG. 4. Superlattice plane $b_\phi = 0.125$.

been prepared correctly. The ideal structure of $CaZr_4O_9$ was then obtained by substituting Ca^{2+} ions and oxygen vacancies on the appropriate sites, as suggested by the data of Allpress *et al.* (*6*).

Initial attempts to minimize the lattice energy of this phase using the shell model resulted in a failure; this was because of polarization difficulties and not due to errors in the input structure, which had been checked as discussed above. We thus adopted a two-step procedure to equilibrate all the coordinates of $CaZr_4O_9$. We started with a "rigid ion" calculation, which does not allow ion polarizability (by excluding core–shell interactions) and thus makes the calculations more straightforward since the unit cell contents are effectively halved.

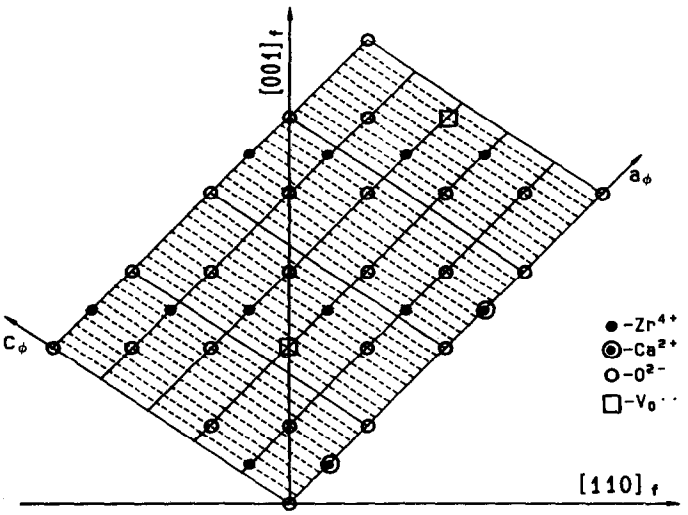

FIG. 5. Superlattice plane $b_\phi = 0.250$.

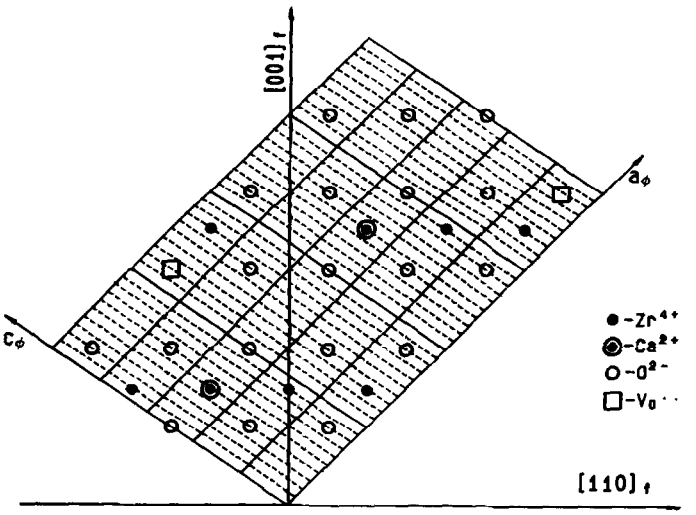

FIG. 6. Superlattice plane $b_\phi = 0.375$.

Once this model was minimized successfully, the complete shell model calculation was performed, but using the rigid ion equilibrium structure as input.

The final equilibrium structure is given in Table IV where it is compared to the input structure and the refined structure of $CaHf_4O_9$. Note that we are able to calculate the coordinates of the oxygen ions, which was not possible from the X-ray analysis of $CaHf_4O_9$. It will be interesting to compare our predicted coordinates with those obtained by a detailed analysis of the structure of the $CaZr_4O_9$ when it becomes available.

The final equilibrated lattice energy of $CaZr_4O_9$, after complete removal of lattice and bulk strains is found to be -7596.312

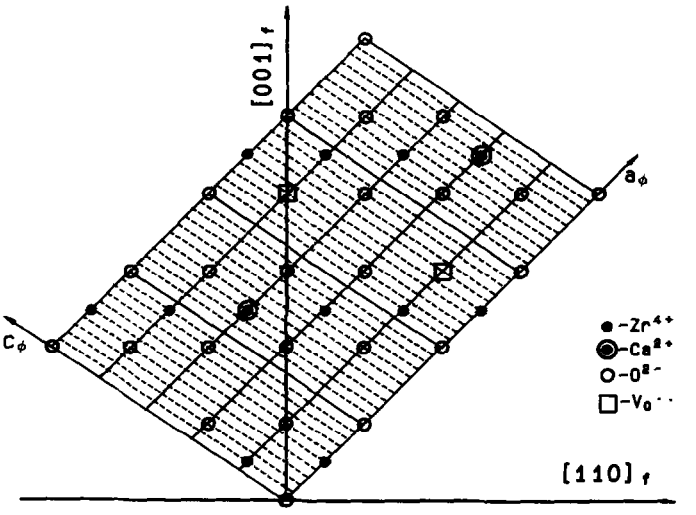

FIG. 7. Superlattice plane $b_\phi = 0.500$.

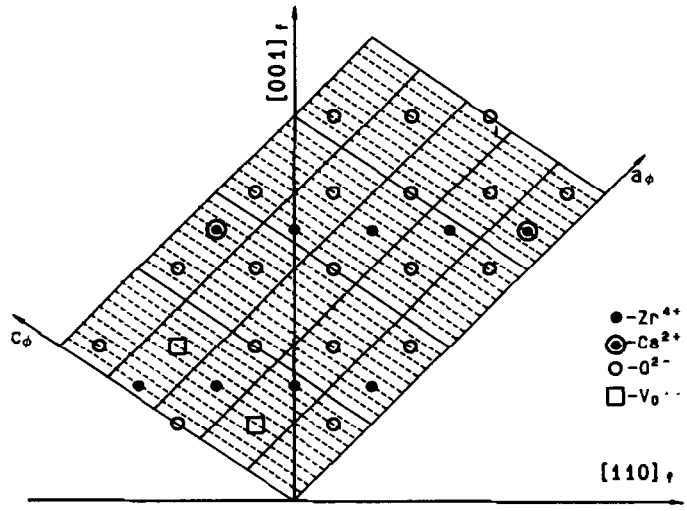

FIG. 8. Superlattice plane $b_\phi = 0.625$.

eV. The formation of $CaZr_4O_9$ from individual oxides can be expressed by Reaction 8. The energy of this reaction, as shown in Eq. (9), is found to be very slightly negative. The very small reaction energy suggests that $CaZr_4O_9$ is not thermodynamically very stable:

$$CaO + 4ZrO_2 \rightarrow CaZr_4O_9 \quad (8)$$

$$E_{\text{reaction}} = (E_{\text{Lattice}}^{CaZr_4O_9})/16 - (E_{\text{Lattice}}^{CaO})/4 - E_{\text{Lattice}}^{ZrO_2} = -0.032 \text{ eV}. \quad (9)$$

In $CaZr_4O_9$ the dopant cations and anion vacancies become ordered. The same amount of CaO can possibly be accommodated in two other ways; one in which the isolated defects Ca''_{Zr} are formed as is de-

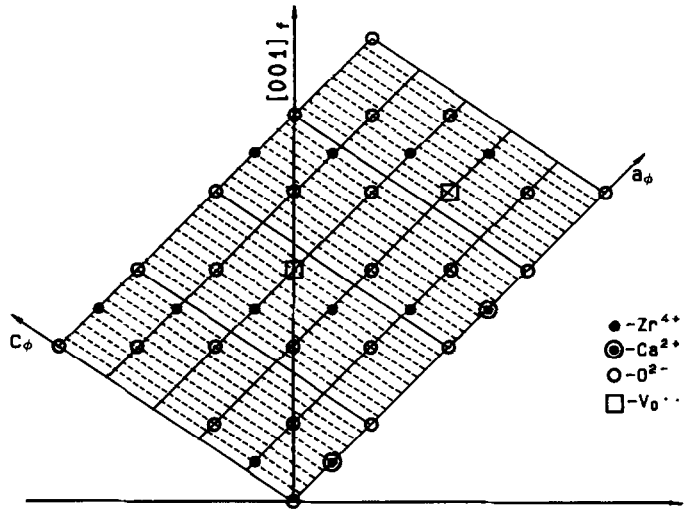

FIG. 9. Superlattice plane $b_\phi = 0.750$.

TABLE IV

COMPARISON OF IONIC COORDINATES IN $CaHf_4O_9$ (6) AND $CaZr_4O_9$ (PRESENT STUDY)

Atom	Site	Ideal Fluorite [6]			$CaHf_4O_9$ [6]			$CaZr_4O_9$ (Present study)		
		x_f	y_f	z_f	x	y	z	x	y	z
Hf/Zr (1)	4(e)	0.0	0.1875	0.25	0.000	0.190_4	0.250	0.0000	0.1838_5	0.2500
Hf/Zr (2)	4(e)	0.5	0.1875	0.25	0.500	0.183_4	0.250	0.5000	0.1877_1	0.2500
Hf/Zr (3)	8(f)	0.4	0.1875	0.45	0.395_3	0.179_3	0.457_3	0.4005_6	0.1896_4	0.4497_6
Hf/Zr (4)	8(f)	0.9	0.1875	0.45	0.891_3	0.178_3	0.456_3	0.8854_1	0.1877_5	0.4431_1
Hf/Zr (5)	8(f)	0.8	0.1875	0.65	0.804_3	0.194_3	0.669_3	0.8101_2	0.1833_8	0.6648
Hf/Zr (6)	8(f)	0.6	0.0625	0.55	0.595_2	0.077_3	0.546_3	0.5936_2	0.0655	0.5466_1
Hf/Zr (7)	8(f)	0.1	0.0625	0.55	0.105_3	0.057_3	0.552_3	0.1027_3	0.0530_3	0.5592_5
Hf/Zr (8)	8(f)	0.7	0.0625	0.35	0.697_3	0.052_2	0.363_3	0.6976_5	0.0598	0.3625_9
Hf/Zr (9)	8(f)	0.2	0.0625	0.35	0.187_3	0.064_2	0.338_4	0.1983_4	0.0651_2	0.3499_6
Ca (1)	4(e)	0.0	0.0625	0.75	0.000	0.053_{14}	0.750	0.0000	0.0614	0.7500
Ca (2)	4(e)	0.5	0.0625	0.75	0.500	0.060_{14}	0.750	0.5000	0.0664_7	0.7500
Ca (3)	8(f)	0.3	0.1875	0.65	0.310_{10}	0.182_9	0.643_{12}	0.3004_6	0.1878_8	0.6474_5
O (1)	8(f)	c	c	c	–	–	–	0.1031_9	0.1738	0.2173_3
O (2)	8(f)	c	c	c	–	–	–	0.3684_7	0.1698_5	0.2630_9
O (3)	8(f)	c	c	c	–	–	–	0.7770_4	0.1593_5	0.4822_2
O (4)	8(f)	c	c	c	–	–	–	0.5257_2	0.2102_9	0.4836_7
O (5)	8(f)	c	c	c	–	–	–	0.2822_4	0.1643_2	0.4241_5
O (6)	8(f)	c	c	c	–	–	–	0.4366_2	0.2192_4	0.6244_6
O (7)	8(f)	c	c	c	–	–	–	0.1380	0.1811	0.6274_2
O (8)	8(f)	c	c	c	–	–	–	0.9168_7	0.2102_3	0.6557_6
O (9)	8(f)	c	c	c	–	–	–	0.6933_9	0.2013_5	0.6379_5
O (10)	8(f)	c	c	c	–	–	–	0.1375_7	0.0529_8	0.7554_1
O (11)	8(f)	c	c	c	–	–	–	0.1300_2	0.4597_4	0.2299_9
O (12)	8(f)	c	c	c	–	–	–	0.0437_5	0.4357_5	0.4961_1
O (13)	8(f)	c	c	c	–	–	–	0.7968_8	0.4741_6	0.4405_2
O (14)	8(f)	c	c	c	–	–	–	0.5373_8	0.4272_1	0.4886_5
O (15)	8(f)	c	c	c	–	–	–	0.2870_7	0.4571	0.4643_7
O (16)	8(f)	c	c	c	–	–	–	0.4312_9	0.4133_7	0.6221_4
O (17)	8(f)	c	c	c	–	–	–	0.9255_3	0.4122_5	0.6321
O (18)	8(f)	c	c	c	–	–	–	0.2970_8	0.4278_5	0.8191_7

[c] The twenty 8(f) anion sites, reported in Ref. (6), have coordinates ($x_f \pm 0.125$, y_f, z_f), where (x_f, y_f, z_f) are the ideal fluorite coordinates of the cations. Eighteen of these sites are reported to be occupied by oxygen and two, V(1) and V(2) as given below, are reported to be vacant. V(1)–8(f): $x_f = 0.025$, $y_f = 0.1875$, $z_f = 0.45$; V(2)–8(f): $x_f = 0.325$, $y_f = 0.0625$, $z_f = 0.35$.

scribed by Reaction 10 and another in which the dopant vacancy associate is formed as described by Reaction 11:

$$CaO + 4ZrO_2 \rightarrow Ca''_{Zr} + V_O^{\cdot\cdot} + 9O_O + 4Zr_{Zr}, \quad \Delta E = 0.881 \text{ eV} \quad (10)$$

$$CaO + 4ZrO_2 \rightarrow [Ca''_{Zr} \cdot V_O^{\cdot\cdot}]^{\times} + 9O_O + 4Zr_{Zr}, \quad \Delta E = 0.204 \text{ eV}. \quad (11)$$

The energy of Reaction 8 is lowest among these three and thus indicates that phase $CaZr_4O_9$ is more likely to form in this sys-

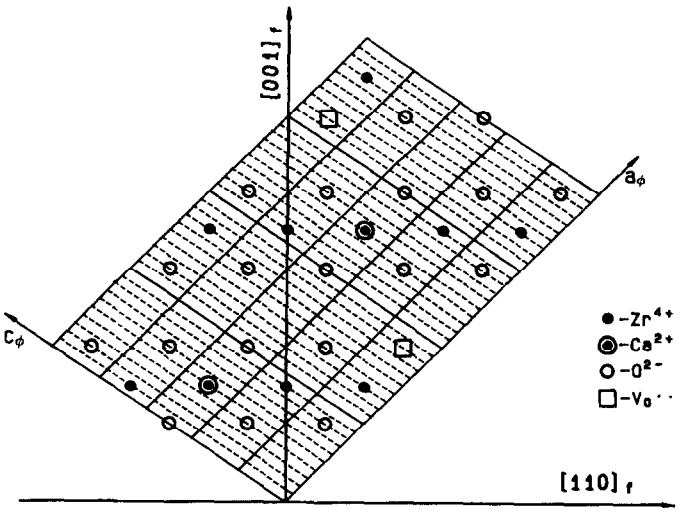

FIG. 10. Superlattice plane $b_\phi = 0.875$.

tem rather than simple aggregates of dopant-vacancy pairs. The energy of Reaction 8 implies that the overall driving force for the formation of this phase in $CaO–ZrO_2$ system is, however, very small. This provides a quantitative basis for the very long annealing times needed to observe this phase in the phase equilibria studies of Hellmann and Stubican (*1*).

Notwithstanding this, the results in Reaction 9 coupled with the energies of Reactions 10 and 11 imply that the ordering into microdomains is a real possibility, at least in the regions of limited spatial extent, since the energy of interaction between $[Ca''_{Zr} \cdot V_O^{\cdot\cdot}]$ complexes to order into microdomains of $CaZr_4O_9$, which is essentially the difference between the energies of these reactions (9 and 11), is quite large.

3.2 $CaZrO_3$

Calculated lattice energy and other lattice properties are reported in Table V. The energy of the reaction which denotes the formation of phase $CaZrO_3$ is

$$CaO + ZrO_2 \rightarrow CaZrO_3, \qquad \Delta E = -0.926\text{eV}. \quad (12)$$

Energies of formation of some isolated point defects in this phase were also calculated and are reported in Table VI. The negative value of Reaction 12 indicates that the reaction is favorable and thus the phase $CaZrO_3$ is expected to form in commercial CSZ, after longer times, especially when the dopant concentration is high.

The calculated equilibrated coordinates are compared with that reported in the literature based on XRD data in Table VII. Agreement is not as good as we hoped for; this is because the potentials do not reflect the change in coordination of the cations in this structure. The potential could be modified in the manner described previously by Cormack *et al.* (*30*) for changes in coordi-

TABLE V

PROPERTIES OF PHASE $CaZrO_3$

Property	Calculated	Observed	
Lattice parameter a_0 (Å)	5.667	5.762	Ref. (29)
Axial ratio b/a	1.386	1.392	Ref. (29)
Axial ratio c/a	0.973	0.970	Ref. (29)
Dielectric constant	15.37	—	—
Elastic constant C_{11} (10^{10} N/m^2)	34.35	—	—
Lattice energy (eV)	−586.286	—	—

TABLE VI

ENERGIES OF SOME FUNDAMENTAL DEFECTS IN PHASE $CaZrO_3$

Defect type	Defect energy (eV)
$[V_{Zr}]''''$	85.729
$[V_{Ca}]''$	20.843
$[V_{OI}]^{\cdot\cdot}$	19.376
$[Ca_{Zr}]''$	62.695
$[Ca_{Zr} \cdot V_O]^{\times}$	Did not converge
$[V_{OII}]^{\cdot\cdot}$	19.365
$[Ca_{Zr} \cdot Zr_{Ca}]^{\times}$	5.517
$Zr_{Ca}^{\cdot\cdot}$	−55.458

nation number, but we did not feel that this would provide any additional insight into the stability of this phase.

The aging of zirconia ceramics may thus be explained on thermodynamic grounds as the formation of microdomains of $CaZr_4O_9$, and in the longer term as the formation of $CaZrO_3$; it is possible, however, that the kinetic factors may hinder the process.

4. Conclusions

The following conclusions may be drawn from the present studies.

TABLE VII

A COMPARISON OF THE FINAL EQUILIBRATED ATOM POSITIONS FROM PRESENT STUDY WITH THE DATA AVAILABLE IN X-RAY LITERATURE (*29*) FOR $CaZrO_3$

Atom	Equilibrated positions (from present study)	Data from literature (X-ray)
Ca 4(c):		
x	0.0030	0.0121
z	0.0148	0.0496
Zr 4(b):	—	—
O(I) 4(c):		
x	−0.0205	−0.0381
z	−0.5727	−0.6032
O(II) 8(d):		
x	0.2849	0.3007
y	0.0374	0.0548
z	0.2859	0.3026

1. $CaZr_4O_9$ has a small driving force to form in the system of present study. The phase $CaZr_4O_9$ has ordered oxygen vacancies which is expected to hinder the migration of oxygen ions. Calculations show that the phase $CaZrO_3$ is likely to form in the CaO–ZrO_2 system. In phase $CaZrO_3$, there are no oxygen vacancies. Thus the transport through these phases is likely to be difficult. Formation of these phases can thus be used to explain the observed fall in electrical conductivity when dopant concentration is high.

2. The charge-compensating oxygen vacancy in the CSZ system is the next nearest neighbor (nnn) rather than the nearest neighbor (nn) to dopant calcium ion, giving it an eightfold coordination and a lower coordination to the zirconium ion sitting at the next cation site. Coupled with our previous results (*16, 17*) of association energies, these results give clear support to the interpretation of the experimental data in terms of microdomain formation, rather than the simple complex proposed by Moringa *et al.* (*11*).

Acknowledgments

We thank the Center for Advanced Ceramic Technology for partial financial support and are grateful to the Cornell National Supercomputer Facility for the provision of computing resources. The CNSF is supported in part by New York State, IBM Corp., and the National Science Foundation.

References

1. J. R. HELLMANN AND V. S. STUBICAN, *J. Amer. Ceram. Soc.* **66**, 260–264 (1983).
2. T. Y. TIEN AND E. C. SUBBARAO, *J. Chem. Phys.* **39**(4), 1041–1047 (1963).
3. J. F. BAUMARD AND P. ABELARD, *in* "Science and Technology of Zirconia II" (A. H. Heuer and M. Richie, Eds.), pp. 555–571 (Adv. in Ceram. Ser.: Vol. 12), Amer. Ceram. Soc., Westerville, OH (1985).
4. R. E. CARTER AND W. L. ROTH, *in* "Electromotive Force Measurements in High Temperature

Systems" (C. B. Alcock, Ed.), pp. 125–144, Institute of Mining and Metallurgy, London (1968).
5. G. BACQUET, J. DUGAS, C. ESCRIBE, AND F. FABRE, *J. Phys. C* **6,** 1432–1442 (1973).
6. J. G. ALLPRESS, J. H. ROSSELL, AND H. G. SCOTT, *J. Solid State Chem.* **14,** 264–273 (1974).
7. B. HUDSON AND P. T. MOSELEY, *J. Solid State Chem.* **19,** 383–389 (1976).
8. D. STEELE AND B. E. F. FENDER, *J. Phys. C* **7,** 1–11 (1974).
9. J. FABER, JR., M. H. MUELLER, AND B. R. COOPER, *Phys. Rev. B* **17**(12), 4884–4888 (1978).
10. M. MORINGA, J. B. COHEN, AND J. FABER, JR., *Acta Crystallogr. Sect. A* **35,** 789–798 (1979).
11. M. MORINGA, J. B. COHEN, AND J. FABER, JR., *Acta Crystallogr. Sect. A* **36,** 520–530 (1980).
12. A. I. GOLDMAN, E. CANOVA, Y. H. KAO, W. L. ROTH, AND R. WONG, *in* "EXAFS and Near-Edge Structure III," pp. 442–447, Springer-Verlag, New York (1984).
13. C. R. A. CATLOW, A. V. CHADWICK, G. N. GREAVES, AND L. M. MORONEY, *J. Amer. Ceram. Soc.* **69**(3), 272–277 (1986).
14. C. R. A. CATLOW, A. V. CHADWICK, A. N. CORMACK, G. N. GREAVES, M. LESLIE, AND L. M. MORONEY, *in* "Defect Properties and processing of High Technology Nonmetallic Materials" (Y. Chen *et al.*, Eds.), Vol. 60, Material Research Society Symposia (1986).
15. A. N. CORMACK, *Mater. Sci. Forum* **7,** 177–186 (1986).
16. A. DWIVEDI, M.S. Thesis, Alfred University, Alfred, NY (1988).
17. A. DWIVEDI, AND A. N. CORMACK, *Philos. Mag.*, to appear (1989).
18. L. M. MORONEY, *Adv. Ceram.* **23,** 649–661 (1987).
19. V. S. STUBICAN AND G. S. CORMAN, *J. Amer. Ceram. Soc.* **68**(4), 174 (1985).
20. B. G. DICK AND A. W. OVERHAUSER, *Phys. Rev.* **112**(1), 90–103 (1958).
21. A. N. CORMACK, *in* "High Technology Ceramics" (P. Vincenzini, Ed.), pp. 351–359, Elsevier, Amsterdam (1987).
22. G. V. LEWIS AND C. R. A. CATLOW, *J. Phys. C* **18,** 1149–1161 (1985).
23. A. N. CORMACK, *Solid State Ionics* **8,** 187–192 (1983).
24. S. C. PARKER, Ph.D. Thesis, University of London, London (1983).
25. M. J. NORGETT AND A. B. LIDIARD, *in* "Computational Solid State Physics" (F. Herman, N. W. Dalton, and T. R. Coehler, Eds.), p. 385, Plenum, New York (1972).
26. W. C. MACKRODT, *in* "Mass Transport in Solids" (F. Beniere and C. R. A. Catlow, Eds.), p. 107, Plenum, New York (1983).
27. A. M. SONEHAM, *in* "Theory of Defects in Solids," Oxford Univ. Press (Clarendon), London/New York (1975).
28. C. R. A. CATLOW, *in* "Lecture Notes in Physics: Computer Simulation of solids" (C. R. A. Catlow and W. C. Mackrodt, Eds.), p. 3, Springer-Verlag, Berlin (1982).
29. H. J. A. KOOPMANS, G. M. H. VAN DE VELDE, AND P. J. GELLINGS, *Acta Crystallogr. C* **39,** 1323–1325 (1983).
30. A. N. CORMACK, G. V. LEWIS, S. C. PARKER, AND C. R. A. CATLOW, *J. Phys. Chem. Solids* **49,** 53–57 (1988).